Computational Materials Science 200 (2021) 110758

Contents lists available at ScienceDirect

Computational Materials Science

journal homepage: www.elsevier.com/locate/commatsci

Quantitative assessment of the role of spin fluctuations in 2D Ising superconductor $NbSe_2$

Suvadip Das *, Igor I. Mazin

[a] Department of Physics and Astronomy and Quantum Science and Engineering Center, George Mason University – Fairfax, VA, USA

ARTICLE INFO

Keywords:
Computational methods
Ising superconductivity
Magnetism in two dimensions
Density functional theory
Materials property
Transition metal dichalcogenides

ABSTRACT

Accurate determination of the full momentum-dependent spin susceptibility $\chi(\mathbf{q})$ is very important for the description of magnetism and superconductivity. While *in principle* the formalism for calculating $\chi(\mathbf{q})$ in the linear response density functional theory (DFT) is well established, hardly any publicly available code includes this capability. Here, we describe an alternative way to calculate the static $\chi(\mathbf{q})$, which can be applied to most common DFT codes without additional programming. The method combines standard fixed-spin-moment calculations of $\chi(\mathbf{0})$ with direct calculations of the energy of spin spirals stabilized by an artificial Hubbard interaction. From these calculations, $\chi_{DFT}(\mathbf{q})$ can be extracted by inverting the RPA formula. We apply this recipe to the recently discovered Ising superconductivity in $NbSe_2$ monolayer, one of the most exciting findings in superconductivity in recent years. It was proposed that spin fluctuations may strongly affect the parity of the order parameter. Previous estimates suggested proximity to ferromagnetism, *i.e.*, $\chi(\mathbf{q})$ peaked at $\mathbf{q} = 0$. We find that the structure of spin fluctuations is more complicated, with the fluctuation spectrum sharply peaked at $\mathbf{q} \approx (0.2, 0)$. Such a spectrum would change the interband pairing interaction and considerably affect the superconducting state.

1. Introduction

Knowledge of the full momentum-dependent spin susceptibility $\chi(\mathbf{q})$ is very important in condensed-matter physics [1]. In particular, it is a key parameter in the theory of spin-fluctuation induced superconductivity [2,3], which has been the subject of intensive research in the last few decades. Moreover, it was recently emphasized that spin fluctuations [4] may play a crucial role in determining the superconducting state property and pairing symmetry even when spin-fluctuations provide a subdominant pairing interaction. This was argued to be the case [5,6] in one of the most exotic recent discoveries in superconductivity, the so-called Ising superconductivity in $NbSe_2$ monolayers [7,8].

Density functional theory (DFT) provides a good starting point, even though in itinerant magnets it overestimates the tendency to magnetism [1]. Unfortunately, calculation of the full spin susceptibility, while conceptually straightforward in DFT, is involved [9], and, most importantly, such capabilities are not included in the common DFT software packages. [10–13] Relatively few publications report such calculations, [14–19], and they are all based on custom-built programs. On the other hand, essentially all popular DFT packages include the capability for fixed spin moment calculations, which provide the exact value for the *uniform* DFT susceptibility $\chi_{DFT}(0)$ at a low computational cost. Comparing thus calculated $\chi_{DFT}(0)$ with the *unrenormalized* one-electron susceptibility $\chi^{(0)}_{DFT}(0) \equiv 2N_F(0)$, where $N_F(0)$ is the density of states per spin at the Fermi level (here and throughout the paper we are using the atomic units convention where the Bohr magneton is chosen to be 1), one can define the so-called Stoner factor I that describes the effect of electron–electron interaction within DFT on the spin susceptibility:

$$\chi_{DFT}(0) = \frac{\chi^{(0)}_{DFT}(0)}{1 - I\chi^{(0)}_{DFT}(0)} \tag{1}$$

Note that, apart from the Umklapp processes this expression is exact in DFT (albeit not in the many-body theory [20]).

While cases are known when the Stoner factor has a non-negligible $\mathbf{q}$ dependence [21], these are uncommon and usually setting I to a $\mathbf{q}$-independent constant is a good approximation. Moreover, following Moriya's Self-Consistent Renormalization Theory [1] one can account for the effect of spin-fluctuations reducing the tendency to magnetism by replacing I with an effective, reduced interaction $I_{eff} = \alpha I$, $\alpha < 1$. This approach is sometimes called *Reduced Stoner Theory* (RST) [22].

* Corresponding author at: Department of Physics and Astronomy, George Mason University, Fairfax VA 22030, USA.
E-mail address: sdas28@gmu.edu (S. Das).

https://doi.org/10.1016/j.commatsci.2021.110758
Received 8 May 2021; Received in revised form 15 July 2021; Accepted 27 July 2021

On the other hand, one can go beyond DFT by adding a local Coulomb interaction, U_{eff}, through the so-called LDA+U method [23]. In fact, it *increases* the tendency to magnetism, rather than decreasing it, as would be required for a better agreement with the experiment in itinerant magnets, but, as we discuss below, gives us a formal tool to calculate $\chi_{DFT}(\mathbf{q})$ without engaging the linear response theory. It was shown that, to a good approximation, this method adds an additional contribution to I, namely κU_{eff}, where the coefficient κ is material dependent and reflects the orbital composition of the states near the Fermi level [24].

In this paper, we propose a simplified way to estimate $\chi_{DFT}(\mathbf{q})$, and, by using RST, the fluctuation-corrected $\chi(\mathbf{q})$, without doing full linear response calculations. The only prerequisite is a DFT package that allows the LDA+U extension (essentially all modern tools do) and spin-spiral calculations (most popular packages such as VASP [10], Elk [11], FLEUR [12], Wien2k [13] have this capability as well). We further illustrate this approach by calculating $\chi_{DFT}(\mathbf{q})$ for the Ising superconductor $NbSe_2$ monolayer.

The paper is organized as follows. First, we present the general theory of the spin susceptibility in the Random Phase Approximation (RPA), which is exact in both DFT and LDA+U. Second, we describe the algorithmic steps to extract $\chi_{DFT}(\mathbf{q})$ for a given $\mathbf{q}$. Finally, we present comprehensive results and relevant discussions for our system of interest, $NbSe_2$ monolayers.

2. General theory

2.1. Spin susceptibility in DFT and beyond

The most general definition of spin susceptibility is given in the real space

$$\chi^{-1}(\mathbf{r},\mathbf{r}') = \frac{\delta^2 E}{\delta m(\mathbf{r})\delta m(\mathbf{r}')}, \tag{2}$$

where E is the total energy of the system. In DFT, it can be written exactly as

$$E = E_1 + E_{xc} + E_{ns} \tag{3}$$

where E_1 is the one-electron energy (sum of the DFT eigenenergies for all occupied states), E_{xc} is the exchange–correlation energy, usually computed in either the Local Density Approximation (LDA) or in the Generalized Gradient Approximation (GGA) [25,26], and E_{ns} does not depend on the spin density. One can then introduce

$$\chi_0^{-1}(\mathbf{r},\mathbf{r}') = \frac{\delta^2 E_1}{\delta m(\mathbf{r})\delta m(\mathbf{r}')} \tag{4}$$

$$I(\mathbf{r},\mathbf{r}') = -\frac{\delta^2 E_{xc}}{\delta m(\mathbf{r})\delta m(\mathbf{r}')} \tag{5}$$

$$\chi_{DFT}^{-1}(\mathbf{r},\mathbf{r}') = \chi_0^{-1}(\mathbf{r},\mathbf{r}') - I(\mathbf{r},\mathbf{r}') \tag{6}$$

Upon Fourier transform, neglecting the Umklapp local field effects [27,20],

$$\chi_{DFT}^{-1}(\mathbf{q}) = \chi_0^{-1}(\mathbf{q}) - I \tag{7}$$

where, as discussed in the Introduction, the $\mathbf{q}$ dependence of I is neglected. Consequently, the RPA approximation [28],

$$\chi_{DFT}(\mathbf{q}) = \frac{\chi_0(\mathbf{q})}{1 - I\chi_0(\mathbf{q})} \tag{8}$$

is exact. The "fixed spin moment" (FSM) method, applicable for $\mathbf{q} = 0$, utilizes Eq. (2) directly:

$$\chi_{DFT}^{-1}(0) = \frac{\delta^2 E}{\delta M^2} = \chi_0^{-1}(0) - I \tag{9}$$

where M is the total magnetization. Modifications described above come as additional terms in this formula

$$\chi_{RST}^{-1}(0) = \frac{\delta^2 E}{\delta M^2} = \chi_0^{-1}(0) - \alpha I \tag{10}$$

where α can be determined from comparison with the experiment, and

$$\chi_{LDA+U}^{-1}(\mathbf{q}) = \frac{\delta^2 E}{\delta M^2} = \chi_{DFT}^{-1}(\mathbf{q}) - \kappa U_{eff}, \tag{11}$$

where $U_{eff} = (U - J)$, as defined in Refs. [23,24].

In principle, one can apply the FSM recipe to finite wave vectors, but very few codes allow frozen spin-wave calculations with fixed amplitude, and in those that do, it is cumbersome and time-consuming. Alternatively, one can use LDA+U and Eq. (11) to extract $\chi_{DFT}^{-1}(\mathbf{q})$ from the instability condition:

$$\chi_{DFT}^{-1}(\mathbf{q}) - \kappa U_{eff} = 0, \tag{12}$$

The recipe is then to vary U_{eff} until the nonmagnetic solution becomes unstable. As mentioned, κ can be determined by applying Eq. (11) at $\mathbf{q} = 0$ and comparing with standard FSM calculations.

One *caveat* is in place. While the above equations deal with infinitesimally small magnetic moments, in reality meta-magnetic states with two metastable solutions, at $M = 0$ and at a finite M may exist. The way to deal with this situation is to always start calculations from a very small moment, making sure that even if the $M = 0$ is not the ground state, the program does not leave this minimum as long as it remains metastable.

2.2. Enhancement of Stoner exchange using DFT+U in the spin susceptibility

The instability of the paramagnetic ground state is dictated by the Stoner criterion for ferromagnetism [29], indicative of strong electron–electron interactions in the system. The latter can be tuned, in a simple way, by including additional on-site interactions in form of the standard Hubbard model in the static mean field approximation, known as "LDA+U" (or, more correctly, DFT+U) method. While DFT underestimates the tendency to magnetism in strongly localized electronic systems, DFT+U compensates for that by incorporating the orbital-selective Hubbard interaction of the strongly localized electrons. In our study, we use the spherically averaged and rotationally invariant LDA+U methodology proposed by Dudarev et al. [23].

$$E_{LSDA+U} = E_{LSDA} + \frac{(U-J)}{2}\sum_{\sigma}(n_{m,\sigma} - n_{m,\sigma}^2) \tag{13}$$

$$= \frac{(U-J)}{2}\sum_{\sigma}\mathrm{Tr}(\rho_\sigma) - \mathrm{Tr}(\rho_\sigma\rho_\sigma) \tag{14}$$

where U and J are the spherically averaged Hubbard repulsion and intra-atomic exchange for electrons with the given angular momentum l, $n_{m,\sigma}$ is the occupation number of the mth orbital, and σ is the spin index. The magnetic interactions can then be efficiently tuned by adding an effective Hubbard parameter $U_{eff} = (U - J)$ as shown by Petukhov et al. [24]. Note that the orbital selective contribution of the effective Hubbard term $U_{eff} = (U - J)$ plays an important role in determining the Stoner factor within the Density Functional Theory framework. Utilizing DFT, the Stoner parameter I can be expressed as $I = -\partial^2 E_{xc}/\partial M^2$, the second derivative of the exchange–correlation energy with respect to the total magnetic moment. The paramagnetic ground state becomes unstable when $\chi_0 I = 2N_F I \geqslant 1$. Upon incorporation of the orbital dependent

Hubbard U parameter, there is an enhancement of the Stoner factor compared to DFT. Within the "fully localized limit" (FLL), the correction to the total energy due to the *DFT* $+U$ can be written as [24]

$$\Delta E^{FLL}_{LDA+U} = -\frac{(U-J)}{2}\sum_{\sigma}\mathrm{Tr}(\rho^{\sigma}.\rho^{\sigma}) - (2l+1)n^{\sigma} \tag{15}$$

This results in an additional contribution to the Stoner parameter

$$\Delta I = \frac{(U-J)}{2N_F^2}\mathrm{Tr}(D{\cdot}D) \tag{16}$$

where $D_{mm'} = -\pi^{-1}ImG_{mm'}(E_F)$ is proportional to the imaginary part of the corresponding Green's function. This additional contribution is proportional to the effective Hubbard term $U_{eff} = (U-J)$, and to the factor, $Tr(D{\cdot}D)$, which depends on the orbital composition of the bands at the Fermi level, and usually can be safely chosen to be a **q**-independent constant, for a given system, thus the additional term can be simply written as $\Delta I = \kappa U_{eff}$.

2.3. Spin-spiral calculations

It was pointed out about 30 years ago by L. M. Sandratskii [30–32] that when solving a single-particle Scrödinger equation in a spiral magnetic field (not necessarily commensurate with the periodicity of the charge potential) a generalized Bloch theorem can be derived, along the following lines:

Let us assume that the spin density in a given unit cell is related to that in all other unit cells as below:

$$\mathbf{M}(\mathbf{r}+\mathbf{R}) = \begin{pmatrix} M_x(\mathbf{r})\cos(\mathbf{q}{\cdot}\mathbf{R}) - M_y(\mathbf{r})\sin(\mathbf{q}{\cdot}\mathbf{R}) \\ M_x(\mathbf{r})\sin(\mathbf{q}{\cdot}\mathbf{R}) + M_y(\mathbf{r})\cos(\mathbf{q}{\cdot}\mathbf{R}) \\ M_z \end{pmatrix} \tag{17}$$

The corresponding spinor wavefunction can be expressed as

$$\phi^{SS}_{n\mathbf{k}}(\mathbf{r}) = \begin{pmatrix} u^{\uparrow}_{nk}(\mathbf{r})e^{i(\mathbf{k}-\mathbf{q}/2)\cdot\mathbf{r}} \\ u^{\downarrow}_{nk}(\mathbf{r})e^{i(\mathbf{k}+\mathbf{q}/2)\cdot\mathbf{r}} \end{pmatrix} \tag{18}$$

where u_{nk} are periodic in the unit cell. This theorem allows solving for $\phi^{SS}_{n\mathbf{k}}(\mathbf{r})$ by solving two separate Bloch equations for $\mathbf{k} \pm \mathbf{q}/2$ using any standard electronic structure methodology. As mentioned in the Introduction section, Sandratskii's method is implemented in many standard DFT packages [10,33,11,13].

Two *caveats* are in place. First, this method is not applicable when spin–orbit coupling is important for the energetics of the material concerned (which is not the case in $NbSe_2$, since it couples the spin-up and the spin-down components. However, spin–orbit interaction can be added perturbatively, as it is done, for instance, in FLEUR [12]. Second, for itinerant metals the magnetic ground state (with an enhanced I) is not necessarily an ideal spiral; it may have amplitude variations periodic in **q**. While this does not affect our methodology, which only exploits the properties near the instability, *i.e.*, near $M = 0$, it might be of interest in other cases. In particular, even while in real life, $NbSe_2$ is not magnetic, the ground state in DFT-GGA is a spin density wave (SDW) [34], the fact that is at least of some academic interest, and it was claimed that the DFT ground state is not a spiral but an amplitude-modulated SDW. If that were the case, it would have been rather unusual for weak itinerant magnetic metals (cf. Sr_2RuO_4, where an amplitude SDW is nearly degenerate with the spin-spiral state, but still loses to the latter [35]). In the results section, we discuss what happens as a matter of fact, within the framework of DFT-GGA in the case of $NbSe_2$ monolayer.

2.4. Computational methods

We have employed the generalized gradient approximation (GGA) for the exchange correlation functional and the projector augmented wave method as implemented within the Vienna Ab initio Simulation Package (VASP) Code [10,33]. The VASP electronic structure code does not adopt any particular approximation to either the charge or magnetization density, or electronic potential, thereby allowing for interatomic as well as intra-atomic noncollinearity of the spin density. Calculations using Generalized Gradient Approximation (GGA) and Hubbard U type corrections for localized d electrons (GGA+U) were performed utilizing the Dudarev approach [23] where the difference $(U-J)$ is incorporated as an effective term U_{eff}. The Nb pseudopotential in our calculations includes the 4d and 5s electrons in the valence bands (inclusion of the latter proved to be quite important). The single-particle wave functions were evaluated using a plane-wave energy cutoff of 600 Ry. The spin susceptibility $\chi(\mathbf{q})$ was evaluated on the 6×6 mesh in the irreducible wedge of the Brillouin zone.

3. Results and discussions

Correlated electronic phases in recently popular two-dimensional materials such as CrI_3 [36,37] and VI_3 [38], exhibit long-range magnetic order in spite of its suppression by thermal fluctuations by virtue of the Mermin-Wagner theorem [39,40]. Among the prospective quantum materials [41–44], bulk 2H-$NbSe_2$ has gained significant popularity due to the simultaneous observation of superconductivity [45] and charge density wave (CDW) [46,47]. The CDW transition in 2H-$NbSe_2$ has been addressed several times computationally [46,47] using the fact that the commensurate charge density wave vector $\mathbf{q} = (1/3, 0)\mathbf{a}^*$ corresponds to a structural reconstruction within a 3×3 supercell ($\mathbf{a}^* = 2\pi/\sqrt{3}a$ is the reciprocal lattice vector). $NbSe_2$, a layered van der Waals material, has recently inspired the study of superconductivity in its monolayer form [48,49,7,50,8]. The proximity effect and magnetic switching at interfaces of this material with other magnetic monolayer TMDs [51,6] such as TaS_2, $TaSe_2$ and $CrBr_3$ warrant detailed study of the low-energy properties in this material. The lack of inversion symmetry in monolayers of 2H-$NbSe_2$ leads to a broken Kramer's spin degeneracy and large spin–orbit (SO) splitting of the states at the momentum K, and its inversion partner, $K' = -K$, in the Brillouin zone. The magnitude of SO-splitting in the monolayer is much larger than the superconducting order parameter [5,6]. The combination of SO-coupling and broken inversion symmetry results in locking of the pseudospins at the points K and K' to be parallel to the c-axis of the monolayer. As a result of time-reversal symmetry, the pseudospins at the K and K' points are antiparallel, with degenerate energies. The ensuing novel phenomenon was aptly named "Ising superconductivity" [7,48,49]. In quantum confined monolayers, screening is significantly reduced compared to bulk, leading to enhancement of electronic correlation. In DFT, this leads to a magnetic instability in the undistorted monolayer, which is remedied either by the formation of a charge density wave, or through quantum fluctuations.

In this section, we elucidate the results pertaining to interesting magnetic phases calculated for the monolayer 1H-$NbSe_2$. As shown in Fig. 1, the spin spiral calculations [30,32] were performed for this systems for various spiral vectors **q** over a fine momentum grid across the

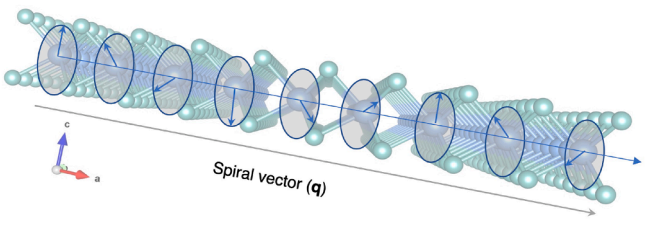

Fig. 1. Graphical representation of the helical spin spiral with the propagation vector $\mathbf{q} = (\pi/3, 0)$ in the monolayer $NbSe_2$. Note that in non-relativistic calculations, the energy does not depend on the orientation of the spin rotation plane.

Table 1
Comparison of the energetics from supercell calculations in monolayer $NbSe_2$ with that of the spin spiral method as implemented in VASP. Note that the energetics of the 5×1, 4×1, 3×1 and 2×1 supercells consistently agree with that of the converged spin spiral calculations, up to a constant shift in energy of 32 meV. E^{ssp}, E_{sup} and $E_{ref} = E_{sup} + 32.132$ meV refers to the spin spiral, supercell and reference energy respectively.

Spin spiral	E_{ssp}(meV)/ f. u.	Supercell	E_{ref}(meV)/ f. u.
$q_1 = 0.2$	−19.818486	5×1	−19.786354
$q_1 = 0.25$	−19.817846	4×1	−19.785754
$q_1 = 0.333$	−19.816859	3×1	−19.784854
$q_1 =$ 0.5(AFM)	−19.817072	2×1	−19.785280

entire irreducible Brillouin zone. Note that the spiral vectors are defined so that the magnetic moment associated with the atomic positions in the atomic lattice have no amplitude along the longitudinal direction of propagation of spiral [30,32], hence excluding magnetic patterns with nonzero net magnetization. Thus this arrangement corresponds to either helical or cycloidal spin spiral (which have, in the absence of spin–orbit, the same energy). For test purposes, we have performed supercell calculations for selected spiral wave vectors. Specifically, we have generated supercell that allowed us to calculate commensurate spirals with $\mathbf{q} = (q_1, 0)$, where $q_1 = \frac{1}{5}, \frac{1}{4}, \frac{1}{3}$ and $\frac{1}{2}$. The comparison of total energies per formula unit for the different spin orientations as obtained from the calculations are presented in Table 1. Apart from a constant energy shift of 32.13 meV the spin spiral calculations fully agree with those in the supercells. Either way, we recognize the DFT ground state to be a spiral with $\mathbf{q} \approx (0.2, 0)$. A previous investigation of magnetic ordering in the monolayer $NbSe_2$ suggested [52] the lowest energy phase to be nearly collinear antiferromagnetic (without a CDW) corresponding to the 4×1 supercell. However, our calculations find this state to be still higher in energy than the $(\frac{1}{5}, 0)$ spiral.

In Fig. 2, we display the lattice structure of a single layer of $NbSe_2$ as viewed from above (along the c-direction) [53]. Note that the Nb atoms are bonded to the adjacent Se atoms in a trigonal prismatic coordination. In order to study the magnetic phases in monolayer $NbSe_2$, constrained fixed spin moment (FSM) calculations were performed where the magnetic moment of the monolayer is varied and the energy difference of the magnetic and nonmagnetic states is calculated. We then fit the calculated total energy as a function of magnetization:

$$E(M) = a_0 + a_1 M^2 + a_2 M^4 + a_3 M^6 + \cdots. \tag{19}$$

and use Eq. (9) to determining the uniform spin susceptibility $\chi_{DFT}(\mathbf{q} = 0)$ from the fitting parameter a_1. From the FSM calculations at $U_{eff} = 0$ we find $\chi_{DFT}(\mathbf{q} = 0) = 6.87 \times 10^{-4}$ emu/mol.

Next, we perform FSM calculations for different values of U_{eff} (Fig. 4). At some values of U_{eff} (in this plot, $U_{eff} = 0.7$ eV) the curve $E(M)$ has two minima, $M = 0$ and another one at a finite moment. One of these minima corresponds to the ground state, and the other to a metastable solution [54]. Either way, for the purpose of determining the susceptibility, we need to know the behavior at small M.

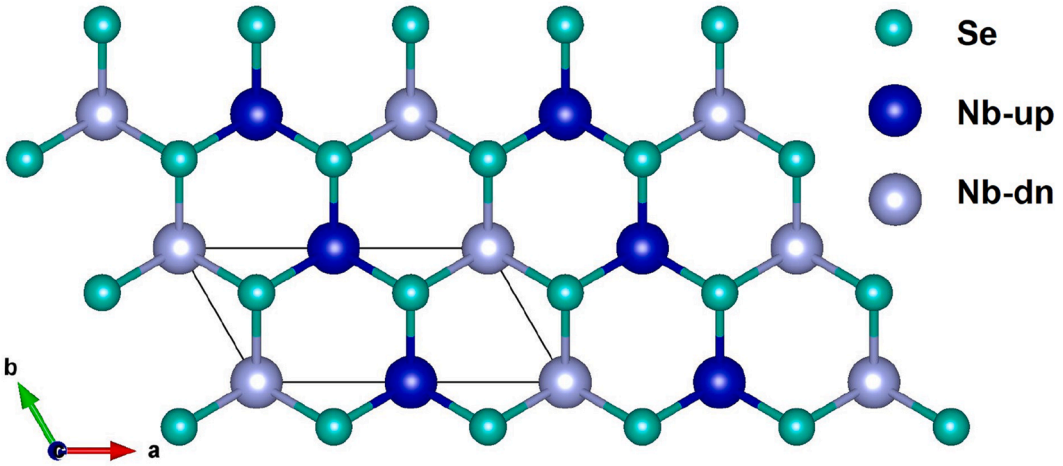

Fig. 2. The crystal lattice structure of monolayer $NbSe_2$ as observed from the top (c-direction). While various magnetic ordering of the material are explored, here we show the prototypical up and down sublattices in the antiferromagnetic configuration.

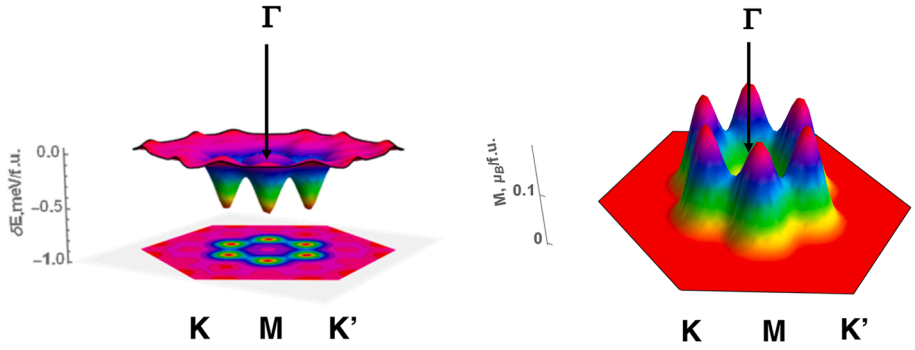

Fig. 3. (a) Energies of the spin spiral states across the Brillouin zone (BZ) of monolayer $NbSe_2$. In order to avoid spurious visual effects at the edges, we show only 86% of the entire Brillouin zone. Note that outside of the narrow regions near $\mathbf{q} = (0.2, 0)$ the spiral calculations collapse, so the energy difference is zero (apart from some numerical noise introduced by the plotting software). (b) Same, for the magnitude of the magnetic moment calculated for the spin spiral.

From the full $E(M)$ curve at each U_{eff} we can find a_1, and we observe that, at the critical value $U_c = 0.918$, a_1 becomes zero and the uniform $\mathbf{q} = 0$ state becomes unstable against ferromagnetism (Fig. 4 (b)). Comparing the already known value of $\chi_{DFT}(\mathbf{q} = 0)$ with the $U_c = 0.918$ and using Eq. (12), we can find the constant κ in that equation, $\kappa = 1.586 \times 10^3$ mol/emu.

Now we are ready to address the spiral states. The calculated energy and magnetic moment at a uniform k-point mesh of spiral vectors $\mathbf{q}$ are presented in Fig. 3. Fig. 3 (a) elucidates the energy spectrum obtained from accurate spin spiral calculations presented as a color map for the entire 2-D hexagonal Brillouin zone. Note that the spin spiral calculations with spiral vectors $\mathbf{q} = \frac{1}{5}\mathbf{a}^*$ correspond to the 5×1 supercell of monolayer $NbSe_2$. Our calculation indicates a sharp energy minimum at this spiral vector, $\mathbf{q} = \frac{1}{5}\mathbf{a}^*$, where the spiral magnetic moment also exhibits a maximum. That is to say, even though the actual material is not magnetically ordered, it is liable to have strong spin fluctuations at and near $\mathbf{q}_c = (0.2, 0)$. The calculated DFT magnetic moment [Fig. 3 (b)] is nonzero in a narrow region near $\mathbf{q}_c$. Our supercell calculations confirm the existence of magnetic instability at this particular wave vector.

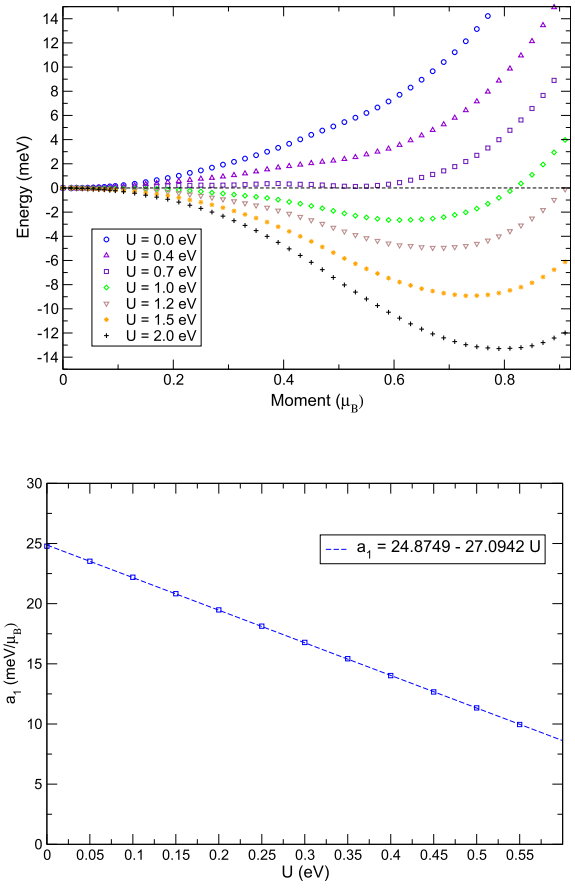

Fig. 4. (a) Fixed spin moment calculation (FSM) for the uniform magnetization $\mathbf{q} = 0$, for various effective Hubbard interaction values ranging from $U_{eff} = 0$ to $U_{eff} = 2.0$ and (b) determination of the critical value $U_{eff} = 0.918$ from the slope of $a_1(U_{eff})$ from the magnetic instability condition.

So far we have discussed unenhanced and unrenormalized DFT calculations. Next, we report energies from spin spiral calculations with an artificially enhanced Hubbard interaction. [23].

Available electronic structure codes [10–12] do not allow FSM calculations for nonzero spiral vectors. Instead, in order to find the critical values $U_c(\mathbf{q})$ corresponding to the onset of an instability, we start calculations from a very small initial magnetic moment of 0.01 μ_B and monitor whether the magnetization will remain on the level of computational noise, or converge to a finite magnetic moment. Starting from a sizeable M_0 for some spiral vector actually leads to a magnetic instability with a finite self-consistent M, even though the $M = 0$ state remains metastable and the susceptibility finite. Of course, such solutions are of no use for determining the susceptibility.

For spiral vectors close to $\mathbf{q} = (0.2, 0)$ the nonmagnetic solution is unstable even for $U_{eff} = 0$. In those cases, we were adding a *negative* U_{eff}. While negative values of U_{eff} are nonphysical, they provide us with an instrument to extract the unrenormalized DFT susceptibilty $\chi_{DFT}(\mathbf{q}) = 1/\kappa U_c(\mathbf{q})$, which, in those cases, is negative. Fig. 5 (a) shows U_c as a function of $\mathbf{q}$ in the 2D hexagonal Brillouin zone. It varies from -1.0 eV at $\mathbf{q} = (0.2, 0)$ to 6.0 eV at the Brillouin zone edge K. We do not plot $\chi_{DFT}(\mathbf{q})$, since it is just inversely proportional to $U_c(\mathbf{q})$ plotted in Fig. 5 (a).

Our next step is to renormalize the DFT spin susceptibilities in the spirit of Moriya's theory [1,22]. As we already know, $\chi_{DFT}(\mathbf{q} = 0) = 6.87 \times 10^{-4}$ emu/mol., while the non-interacting susceptibility $\chi_0 = 0.872 \times 10^{-4}$ emu/ mol., from the density of states at the Fermi level $N(0) = 2.7$ states/f.u. and the DFT Stoner factor can be calculated to be $I = 0.323$ eV/f.u. (or 0.646 eV/f.u. spin) Now, applying Eq. (12) to the magnetic instability corresponding to spiral vector $\mathbf{q} = 0$ and critical effective Hubbard interaction $U_{eff} = 0$ yields $\kappa = 1.56 \times 10^3$ (mol/emu)/eV ($\mathrm{Tr}(D{\cdot}D)/2N_F^2 = 0.1$ in Eq. (16)).

Following the formalism for Reduced Stoner Theory [24], we introduce the fluctuation-induced Moriya factor α, so that $I_{eff} = \alpha I, \alpha < 1$. Using

$$\chi^{-1}_{RST}(\mathbf{q}) = \chi^{-1}_{DFT}(\mathbf{q}) + (1 - \alpha)I \tag{20}$$

we can determine α by comparing Eq. (20) with the experimental spin

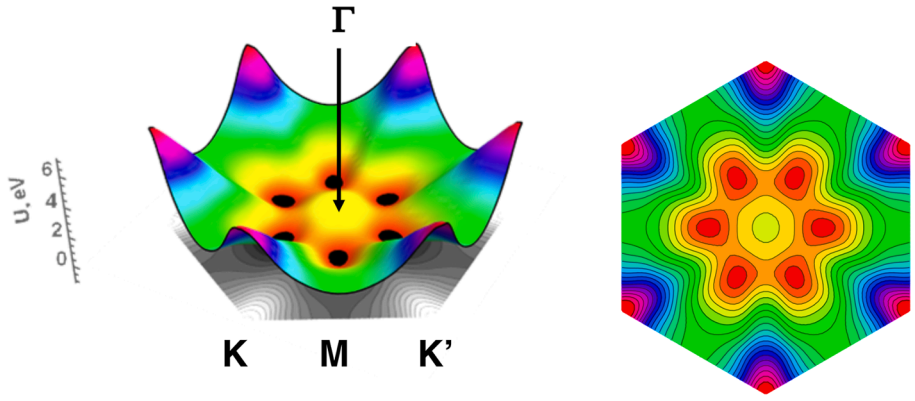

Fig. 5. (a) Critical value of effective Hubbard interaction U_{eff} defining the magnetic instability as a function of the spiral vector $\mathbf{q}$ across the entire Brillouin zone of monolayer $NbSe_2$ and (b) the corresponding contour plot, of U_{eff}, as viewed from above.

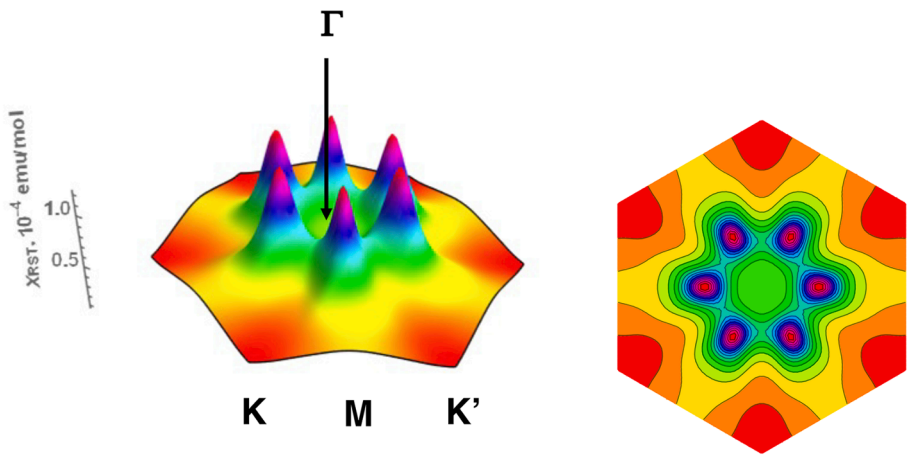

Fig. 6. The figure shows (a) the fluctuation-renormalized spin susceptibility as a function of the spiral vector $\mathbf{q}$ across the entire Brillouin zone of monolayer $NbSe_2$, and (b) the corresponding contour plot, of $\chi_{RST}(\mathbf{q})$, as viewed from above.

susceptibility, if the latter is available. As of now, the experimental spin susceptibility has been measured only for the bulk sample of $NbSe_2$ [55]. The bulk experimental and first principles spin susceptibilities for $\mathbf{q} = 0$ are $\chi_{expt} = 3 \times 10^{-4}$ emu/mol. and $\chi_{DFT} = 4.28 \times 10^{-4}$ emu/mol. Assuming the contribution from spin fluctuations in monolayer to be the same, we use $\alpha = 0.891$. Utilizing this α and $\chi_{DFT}(\mathbf{q})$, we obtain the fully renormalized q-dependent spin susceptibility for monolayer $NbSe_2$, shown in Fig. 6 as a function of the spiral vector $\mathbf{q}$. Note that we observe two maxima, a weak peak around the Γ point and the principal set of peaks around six points equivalent to $\mathbf{q} = (0.2, 0)$.

Let us now briefly discuss ramifications of these findings for superconductivity. As discussed in Ref. [5], an Ising material like $NbSe_2$ behaves as a singlet superconductors only when the amplitude of the order parameter on the two spin–orbit split Fermi surfaces is exactly the same. Ref. [5] argued that it is not the case in $NbSe_2$ even for a purely phonon-driven superconductivity[56]. In a future paper we will present a full anisotropic Eliashberg solution for the $\mathbf{k}$-dependent order parameter including both phonons and spin fluctuations, below we will give a semiquantative estimate of the effect of the later.

SF-induced pairing fluctuation is directly proportional to the spin susceptibility. Since the calculated $\chi_{RST}(\mathbf{q})$ shows very sharp peaks at $\mathbf{q_0} = (0.2, 0)$ and equivalent vectors, it can be, in the first approximation, treated as a constant for all $\mathbf{q}$ such that $|\mathbf{q} - \mathbf{q}_0| < \delta q, \delta q \ll q_0$ While SF generate pair interaction in both intraband and interband channel, the later does not affect the ratio of the order parameter (as long as the DOS on both spin–orbit split bands are the same). The coupling constant is then, up to a constant factor, $\delta q / \pi k_F$, which gives us the fraction of each Fermi surface affected by this interaction. Here, k_F is the average Fermi momentum for each surface. For $NbSe_2$ single layer, the ratio of the inner and outer Fermi momenta is on the order of 30% [5], and that is how much the reduction of the order parameter due to spin fluctuations will differ for the two bands. One should keep in mind that SF in this case are a *subdominant* interaction, reducing the order parameter generated by the electron–phonon coupling, so the 30% reduction in the SF coupling strength will not translate into a 30% change in the *total* coupling – but it will still be a sizable effect. Future calculation with full Eliashberg equations including both types of interactions will give an ultimate answer to the actual fraction of the triplet admixture.

4. Summary and conclusions

In summary, we have designed a protocol to estimate both DFT [57,26,58] and fluctuation-renormalized [24,22,20] (in the spirit of Moriya's theory) spin susceptibility, especially well suited for materials close to a magnetic instability, but not surpassing it. The protocol does not require linear-response calculations [14], nor explicit accounting for fluctuations [19,18], as it is done, for instance, in dynamical mean field theory. It is based on the capability to tune a material's propensity to magnetism by including a variable LDA+U correction [23] (even in a weakly correlated material), and then reverse-engineering the standard RPA formula [28].

The formalism includes two *a priori* unknown constants, assumed to be $\mathbf{q}$-independent, one of which can be fixed by a comparison with the fixed spin moment calculations at $\mathbf{q} = 0$, and the other by a comparison with the experimentally observed uniform spin susceptibility. The capabilities to perform FSM calculations at $\mathbf{q} = 0$, and self-consistent spiral calculations at an arbitrary $\mathbf{q}$ are built-in within most standard DFT codes. Thus, our formalism provides a recipe of how to deal with complex situations on the verge of magnetic instability, where the bare DFT can be rather inaccurate.

We apply this procedure to a 2D Ising superconductor, monolayer $NbSe_2$. We find very strong antiferromagnetic spin fluctuation at and near $\mathbf{q} = (0.2, 0)$, indicating that the structure of spin fluctuations in the momentum space in this superconductor is more complicated that previously thought of. These findings have direct ramifications for the structure of the superconducting order parameter in monolayer $NbSe_2$, especially on the degree of the singlet–triplet mixing [6]. These ramifications are discussed qualitatively, while a full quantitative analysis will be presented in a separate publication.

5. Data availability statement

All input files and data generated in this project are available from the authors upon request.

CRediT authorship contribution statement

Suvadip Das: Conceptualization, Methodology, Investigation, Data curation, Writing - original draft, Visualization. **Igor I. Mazin:** Conceptualization, Methodology, Writing - review & editing, Visualization, Supervision.

Declaration of Competing Interest

The authors declare that they have no known competing financial interests or personal relationships that could have appeared to influence the work reported in this paper.

Acknowledgments

The authors acknowledge financial support for their research from

the Office of Naval Research through Grant N00014-20-1-2345. The authors also acknowledge the Department of Defense (DoD) Major Shared Computing Resource Center at Air Force Research Laboratory (AFRL) and the National Energy Research Scientific Computing Center (NERSC) for high-performance computing facilities for significant portion of calculations performed in this work. We thank V. P. Antropov for useful discussions.

References

[1] T. Moriya, Spin Fluctuations in Itinerant Electron Magnetism, Springer Series in Solid-State Sciences, Springer, Berlin Heidelberg, 2012.
[2] N.F. Berk, J.R. Schrieffer, Effect of ferromagnetic spin correlations on superconductivity, Phys. Rev. Lett. 17 (1966) 433–435.
[3] D. Fay, J. Appel, Coexistence of p-state Superconductivity and Itinerant Ferromagnetism, Phys. Rev. B 22 (7) (1980) 3173–3182.
[4] M. Kawamura, Y. Hizume, T. Ozaki, Benchmark of density functional theory for superconductors in elemental materials, Phys. Rev. B 101 (13) (2020) 134511, https://doi.org/10.1103/PhysRevB.101.134511.
[5] D. Wickramaratne, S. Khmelevskyi, D.F. Agterberg, I.I. Mazin, Ising Superconductivity and Magnetism in $NbSe_2$, Phys. Rev. X 10 (2020) 041003, https://doi.org/10.1103/PhysRevX.10.041003.
[6] A. Hamill, B. Heischmidt, E. Sohn, D. Shaffer, K.T. Tsai, X. Zhang, X. Xi, A. Suslov, H. Berger, L. Forró, F.J. Burnell, J. Shan, K.F. Mak, R.M. Fernandes, K. Wang, V.S. Pribiag, Unexpected two-fold symmetric superconductivity in few-layer NbSe2 (2020). arXiv:arXiv:2004.02999.
[7] X. Xi, Z. Wang, W. Zhao, J.-H. Park, K.T. Law, H. Berger, L. Forro, J. Shan, K. F. Mak, Ising pairing in superconducting $NbSe_2$ atomic layers, Nat. Phys. 12 (2) (2016) 139.
[8] T. Dvir, F. Massee, L. Attias, M. Khodas, M. Aprili, C.H.L. Quay, H. Steinberg, Spectroscopy of bulk and few-layer superconducting NbSe2 with van der Waals tunnel junctions, Nat. Commun. 9 (2018) 598.
[9] A.I. Liechtenstein, V.I. Anisimov, J. Zaanen, Density-functional theory and strong interactions: Orbital ordering in Mott-Hubbard insulators, Phys. Rev. B 52 (1995) R5467–R5470, https://doi.org/10.1103/PhysRevB.52.R5467.
[10] G. Kresse, J. Hafner, Ab initio molecular dynamics for liquid metals, Phys. Rev. B 47 (1993) 558–561.
[11] The Elk Code, URL:http://elk.sourceforge.net/.
[12] P. Kurz, F. Förster, L. Nordström, G. Bihlmayer, S. Blügel, Ab initio treatment of noncollinear magnets with the full-potential linearized augmented plane wave method, Phys. Rev. B 69 (2004) 024415.
[13] The WIEN2k Code, URL:http://susi.theochem.tuwien.ac.at/.
[14] S.Y. Savrasov, Linear response calculations of spin fluctuations, Phys. Rev. Lett. 81 (1998) 2570–2573, https://doi.org/10.1103/PhysRevLett.81.2570.
[15] F. Essenberger, P. Buczek, A. Ernst, L. Sandratskii, E.K.U. Gross, Paramagnons in FeSe close to a magnetic quantum phase transition: Ab-initio study, Phys. Rev. B 86 (2012) 060412.
[16] M. Monni, F. Bernardini, G. Profeta, A. Sanna, S. Sharma, J.K. Dewhurst, C. Bersier, A. Continenza, E.K.U. Gross, S. Massidda, Static and dynamical susceptibility of $LaO_{1-x}F_xFeAs$, Phys. Rev. B 81 (2010), 104503.
[17] T. Kotani, M.V. Schilfgaarde, Spin wave dispersion based on the quasiparticle self-consistent GW method: NiO, MnO and α-MnAs, J. Phys.: Condens. 20 (Matter 2008,), 295214.
[18] A.L. Wysocki, A. Kutepov, V.P. Antropov, Strength and scales of itinerant spin fluctuations in 3*d* paramagnetic metals, Phys. Rev. B 94 (2016), 140405.
[19] A.L. Wysocki, V.N. Valmispild, A. Kutepov, S. Sharma, J.K. Dewhurst, E.K.U. Gross, A.I. Lichtenstein, V.P. Antropov, Spin-density fluctuations and the fluctuation-dissipation theorem in 3*d* ferromagnetic metals, Phys. Rev. B 96 (2017), 184418.
[20] I.I. Mazin, R.E. Cohen, Notes on the static dielectric response function in the density functional theory, Ferroelectrics 194 (1) (1997) 263–270.
[21] I.I. Mazin, D.J. Singh, Competitions in layered ruthenates: Ferromagnetism versus antiferromagnetism and triplet versus singlet pairing, Phys. Rev. Lett. 82 (1999) 4324–4327.
[22] L. Ortenzi, I.I. Mazin, P. Blaha, L. Boeri, Accounting for spin fluctuations beyond local spin density approximation in the density functional theory, Phys. Rev. B 86 (6) (2012).
[23] S.L. Dudarev, G.A. Botton, S.Y. Savrasov, C.J. Humphreys, A.P. Sutton, Electron-energy-loss spectra and the structural stability of nickel oxide: An LSDA +U study, Phys. Rev. B 57 (1998) 1505–1509.
[24] A.G. Petukhov, I.I. Mazin, L. Chioncel, A.I. Lichtenstein, Correlated metals and the LDA +U method, Phys. Rev. B 67 (2003), 153106.
[25] D.M. Ceperley, B.J. Alder, Ground state of the electron gas by a stochastic method, Phys. Rev. Lett. 45 (1980) 566–569.
[26] J.P. Perdew, K. Burke, M. Ernzerhof, Generalized gradient approximation made simple, Phys. Rev. Lett. 77 (18) (1996) 3865.
[27] I. Mazin, Local field effects in the many-body perturbation theory and in the density functional theory, Preprint ICTP IC-88/196 (1988).
[28] P. Nozières, D. Pines, Electron interaction in solids. characteristic energy loss spectrum, Phys. Rev. 113 (1959) 1254–1267.
[29] S. Blundell, Magnetism in Condensed Matter, Oxford Master Series in Condensed Matter Physics, OUP Oxford, New York, 2001.
[30] L.M. Sandratskii, Symmetry analysis of electronic states for crystals with spiral magnetic order: I. general properties, 1, Phys.: Condens. Matter 3 (1991) 8565–8585.
[31] K. Knöpfle, L.M. Sandratskii, J. Kübler, Spin spiral ground state of γ-iron, Phys. Rev. B 62 (2000) 5564–5569.
[32] L.M. Sandratskii, Noncollinear magnetism in itinerant-electron systems: Theory and applications, Adv. Phys. 47 (1) (1998) 91–160.
[33] The VASP Code, URL:https://www.vasp.at/.
[34] F. Zheng, Z. Zhou, X. Liu, J. Feng, First-principles study of charge and magnetic ordering in monolayer $NbSe_2$, Phys. Rev. B 97 (2018) 081101.
[35] B. Kim, S. Khmelevskyi, I.I. Mazin, D.F. Agterberg, C. Franchini, Anisotropy of magnetic interactions and symmetry of the order parameter in unconventional superconductor Sr2RuO4,, npj Quant. Mater. (2017).
[36] B. Huang, G. Clark, D.R. Klein, D. MacNeill, E. Navarro-Moratalla, K.L. Seyler, N. Wilson, M.A. McGuire, D.H. Cobden, D. Xiao, W. Yao, P. Jarillo-Herrero, X. Xu, Electrical control of 2D magnetism in bilayer CrI_3, Nat. Nanotechnol. 13 (2018) 544–548.
[37] S. Jiang, L. Li, Z. Wang, F.K. Mak, J. Shan, Controlling magnetism in 2D CrI_3 by electrostatic doping, Nat. Nanotechnol. 13 (2018) 549–553.
[38] S. Tian, J.-F. Zhang, C. Li, T. Ying, S. Li, X. Zhang, K. Liu, H. Lei, Ferromagnetic van der waals crystal VI_3, J. Am. Chem. Soc. 141 (13) (2019) 5326–5333.
[39] N.D. Mermin, H. Wagner, Absence of ferromagnetism or antiferromagnetism in one- or two-dimensional isotropic heisenberg models, Phys. Rev. Lett. 17 (1966) 1133–1136.
[40] P.C. Hohenberg, Existence of long-range order in one and two dimensions, Phys. Rev. 158 (1967) 383–386.
[41] J. Li, P. Song, J. Zhao, Z. Li, Z. Qiu, Z. Wang, L. Lin, M. Zhao, T.S. Herng, Y. Zuo, W. Johnson, W. Yu, X. Hai, P. Lyu, H. Xu, H. Yang, C. Chen, S.J. Pennycook, J. Ding, J. Teng, A.H. Castro Neto, K.S. Novoselov, J. Lu, Printable two-dimensional superconducting monolayers, Nat. Mat. 20 (2021) 181–187.
[42] D. Wickramaratne, M. Haim, M. Khodas, I.I. Mazin, Proximity effects and tunneling in an ising superconductor-magnetic insulator heterostructure (2021). arXiv: 2101.12674.
[43] J.M. Lu, O. Zheliuk, I. Leermakers, N.F.Q. Yuan, U. Zeitler, K.T. Law, J.T. Ye, Evidence for two-dimensional Ising superconductivity in gated MoS_2, Science 350 (6266) (2015) 1353–1357.
[44] Y.S. Gani, H. Steinberg, E. Rossi, Superconductivity in twisted graphene $NbSe_2$ heterostructures, Phys. Rev. B 99 (2019), 235404.
[45] T. Yokoya, T. Kiss, A. Chainani, S. Shin, M. Nohara, H. Takagi, Fermi Surface Sheet-Dependent Superconductivity in 2H-NbSe2, Science 294 (5551) (2001) 2518–2520.
[46] M. Leroux, I. Errea, M. Le Tacon, S.-M. Souliou, G. Garbarino, L. Cario, A. Bosak, F. Mauri, M. Calandra, P. Rodière, Strong anharmonicity induces quantum melting of charge density wave in 2H-$NbSe_2$ under pressure, Phys. Rev. B 92 (2015) 140303.
[47] K. Cho, M. Konczykowski, S. Teknowijoyo, M.A. Tanatar, J. Guss, P.B. Gartin, J. M. Wilde, A. Kreyssig, R.J. McQueeney, A.I. Goldman, V. Mishra, P.J. Hirschfeld, R. Prozorov, Using controlled disorder to probe the interplay between charge order and superconductivity in $NbSe_2$, Nat. Commun. 9 (2018) 2798.
[48] Y. Xing, K. Zhao, P. Shan, F. Zheng, Y. Zhang, H. Fu, Y. Liu, M. Tian, C. Xi, H. Liu, J. Feng, X. Lin, S. Ji, X. Chen, Q.K. Xue, J. Wang, Ising superconductivity and quantum phase transition in macro-size monolayer $NbSe_2$, Nano Lett. 17 (11) (2017) 6802–6807.
[49] C. Wang, B. Lian, X. Guo, J. Mao, Z. Zhang, D. Zhang, B.L. Gu, W. Xu, Y.and Duan, Type-II Ising superconductivity in two-dimensional materials with spin-orbit coupling, Phys. Rev. Lett. 123 (2019) 126402.
[50] C.-S. Lian, C. Si, W. Duan, Unveiling charge-density wave, superconductivity, and their competitive nature in two-dimensional $NbSe_2$, Nano Lett. 18 (5) (2018) 2924–2929.
[51] S.C. de la Barrera, M.R. Sinko, D.P. Gopalan, N. Sivadas, K.L. Seyler, K. Watanabe, T. Taniguchi, A.W. Tsen, X. Xu, D. Xiao, B.M. Hunt, Tuning Ising superconductivity with layer and spin-orbit coupling in two-dimensional transition-metal dichalcogenides, Nat. Commun. 9 (1) (2018) 1427.
[52] F. Zheng, Z. Zhou, X. Liu, J. Feng, First-principles study of charge and magnetic ordering in monolayer $NbSe_2$, Phys. Rev. B 97 (2018) 081101.
[53] K. Momma, F. Izumi, VESTA3 for three-dimensional visualization of crystal, volumetric and morphology data, J. Appl. Crystallogr. 44 (6) (2011) 1272–1276, https://doi.org/10.1107/S0021889811038970.
[54] D.I. Khomskii, Basic Aspects of the Quantum Theory of Solids: Order and Elementary Excitations, Cambridge University Press, Leiden, 2010.
[55] M. Iavarone, R. Di Capua, G. Karapetrov, A.E. Koshelev, D. Rosenmann, H. Claus, C.D. Malliakas, M.G. Kanatzidis, T. Nishizaki, N. Kobayashi, Effect of magnetic impurities on the vortex lattice properties in $NbSe_2$ single crystals, Phys. Rev. B 78 (2008), 174518.
[56] Preliminary calculations by R. Margine et al. indicate about 10% difference, yielding a triplet admixture of the order of 10% (unpublished).
[57] D. Hobbs, G. Kresse, J. Hafner, Fully unconstrained noncollinear magnetism within the projector augmented-wave method, Phys. Rev. B 62 (2000) 11556–11570.
[58] G. Kresse, J. Furthmüller, Efficient iterative schemes for ab initio total-energy calculations using a plane-wave basis set, Phys. Rev. B 54 (1996) 11169–11186.